Self-Assembly of Ferromagnetic Organic–Inorganic Perovskite-Like Films

Naureen Akhtar, Alexey O. Polyakov, Aisha Aqeel, Pavlo Gordiichuk, Graeme R. Blake, Jacob Baas, Heinz Amenitsch, Andreas Herrmann, Petra Rudolf, and Thomas T. M. Palstra**

Perovskite-based organic–inorganic hybrids hold great potential as active layers in electronics or optoelectronics or as components of biosensors. However, many of these applications require thin films grown with good control over structure and thickness—a major challenge that needs to be addressed. The work presented here is an effort towards this goal and concerns the layer-by-layer deposition at ambient conditions of ferromagnetic organic–inorganic hybrids consisting of alternating $CuCl_4$-octahedra and organic layers. The Langmuir-Blodgett technique used to assemble these structures provides intrinsic control over the molecular organization and film thickness down to the molecular level. Magnetic characterization reveals that the coercive field for these thin films is larger than that for solution-grown layered bulk crystals. The strategy presented here suggests a promising cost effective route to facilitate the excellently controlled growth of sophisticated materials on a wide variety of substrates that have properties relevant for the high density storage media and spintronic devices.

1. Introduction

Layered organic–inorganic hybrids[1–3] have attracted significant attention due to their versatility for combining various functionalities such as magnetism,[4,5] ferroelectricity,[6–8] and electrical conductivity.[9–13] In particular, self-assembling heterostructures with well-defined smooth interfaces holds great promise for integrated device systems.[14–16] The past few decades have witnessed much activity in building novel hybrid assemblies with useful (multi)functionality.[3,6] However, most of the hybrid materials reported so far have been obtained as (single) crystals. Although single crystals serve as the most efficient medium for exploring and even tuning the structural and physical properties, practical implementation of desired materials in many electronic and optical applications requires the ability to prepare them as thin films. Processing methods that enable the fabrication of interesting materials as thin films with innovative low-cost potential are highly desirable for making inroads into the commercial world.

The work reported here derived inspiration from the report[6] on multiferroicity in $CuCl_4(C_6H_5CH_2CH_2NH_3)_2$ hybrid crystals; these crystals have a layered structure with polar interfaces where buckling of the $CuCl_4$ octahedra, organic block site-shift and NH_3^+ bond reordering play a crucial role in defining the electronic properties.[6] The challenge addressed here is to produce these materials in the form of thin films with tailorable composition and size. Mitzi[17] has demonstrated various techniques for the successful deposition of organic–inorganic thin films via sol–gel, Langmuir-Blodgett (LB) and solution processing.[17,18] Among these techniques, the Langmuir-Blodgett technique takes advantage of the soluble nature of the precursors for these hybrid

Dr. N. Akhtar, A. O. Polyakov, A. Aqeel, P. Gordiichuk, Dr. G. R. Blake, J. Baas, Prof. A. Herrmann, Prof. P. Rudolf, Prof. T. T. M. Palstra
Zernike Institute for Advanced Materials
University of Groningen
Nijenborgh 4, NL-9747AG, Groningen, The Netherlands
E-mail: p.rudolf@rug.nl; t.t.m.palstra@rug.nl
Dr. H. Amenitsch
Institute of Inorganic Chemistry
Graz University of Technology
Strehmayerg. 6/IV A-8010, Graz, Austria

DOI: 10.1002/smll.201400259

materials and provides excellent control down to the molecular level through simple tuning of external parameters during growth.[19,20] Langmuir-Blodgett deposition is a versatile method for thin film growth, not only because of the low processing temperatures but also because it offers the possibility to exploit self-assembly and to use flexible substrates. This method can be used to grow not only organic supramolecular architectures on surfaces but also ultrathin inorganic structures[21] as demonstrated for example by Sugai et al.,[22] who used LB deposition to synthesize $PbTiO_3$ ultrathin films with stearic acid, Pb salts and Ti salt as starting precursors. Contrary to pulsed laser deposition or molecular beam epitaxy, where light organic molecules easily decompose as a result of high temperature processing, the LB technique provides reliable synthesis conditions for the controlled deposition of organic material.[17,23]

The $CuCl_4$-based hybrid family was taken as a bulk-form prototype for the film synthesis.[6,24] Organic and inorganic parts are connected via hydrogen bonds between the NH_3 group and the chlorine ions of corner-shared $CuCl_4$ octahedra. In the case of thin films, we expect the same arrangement. The Langmuir-Blodgett technique implies layer-by-layer synthesis from the solvent-air interface and thus requires amphiphilic organic molecules with terminal cationic groups. As we demonstrate here, when these molecules are spread on the $CuCl_2$ salt containing water surface, this leads to hybrid assembly at the interface through formation of $CuCl_4$ octahedra-based inorganic sheets. Interestingly, this growth method allows the electrical and magnetic properties to be tuned by modifying the interlayer spacing in the multilayer film. Moreover, adding local anisotropy through asymmetric coordination of the inorganic sheets can induce significant changes in the magnetic properties. Hence the architecture of the films is different from that of bulk hybrid crystals, which results in modified physical properties in films relative to their bulk analogues. Comparison of the physical properties of hybrid LB films having asymmetric coordination with those of bulk crystals, where the coordination is symmetric, highlights the role of local anisotropy.

2. Results and Discussion

2.1. Self-Assembly of the Hybrid Langmuir Film

A first step towards the optimization of the quality of a film deposited by the Langmuir-Blodgett technique consists in studying the properties of the Langmuir film assembled at the air-water interface. Pressure-area isotherms, recorded during the compression of the Langmuir film, not only indicate whether a film is formed from the available molecular building blocks, but they also yield crucial information on the molecular packing and the stability of the film. Brewster angle microscopy (BAM), on the other hand, provides a direct real time visualization of the homogeneity and the morphology, as well as highlighting phase changes in the floating film at the water surface. Hybrid Langmuir films were obtained

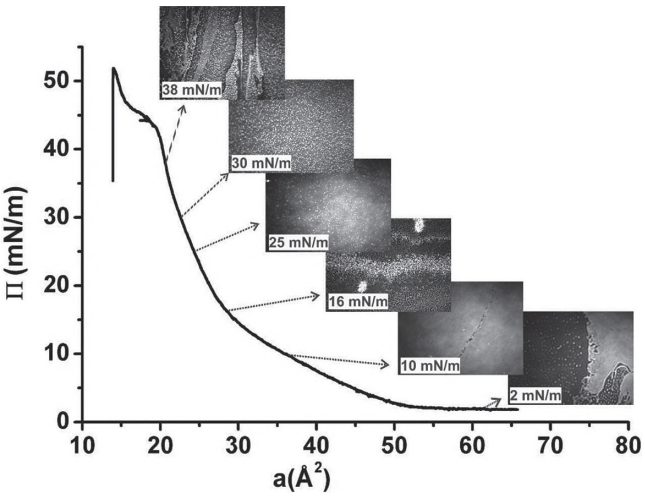

Figure 1. *Π–a* isotherm of $ODAH^+Cl^-$ on an aqueous $CuCl_2$-MA subphase and Brewster angle micrographs taken at various stages during the continuous compression.

by spreading a chloroform-methanol (9:1) solution of octadecyl ammonium chloride ($ODAH^+Cl^-$; 0.15 mg/mL) onto the subphase that was maintained at a temperature of 21 °C. The subphase employed in the experiments was an aqueous solution of copper chloride ($CuCl_2$; 1.0×10^{-3} mol/L) and methyl ammonium chloride (MA; 1.0×10^{-3} mol/L). After a one hour waiting time to allow for solvent evaporation, the molecules were compressed at a rate of 30 $cm^2\ min^{-1}$ by a movable barrier.

Figure 1 displays the surface pressure–area per molecule (*Π–a*) isotherm of $ODAH^+Cl^-$ on the $CuCl_2$-MA subphase along with BAM images taken at various stages during the continuous compression. While the *Π–a* isotherms recorded in a Langmuir trough usually start at $\Pi = 0$, here the isotherm started at an initial surface pressure of ≈2 mN/m. Such a high initial surface pressure in the $ODAH^+Cl^-$ isotherm has also been observed for a $PbCl_2$-MA subphase, as reported by L. Xu et al.,[25] and results from the electrostatic repulsion between $ODAH^+$ and positive metal ions.

The isotherm of the $ODAH^+Cl^-$ layer on pure water gave a lift-off area of ≈30 $Å^2$.[25] The presence of $CuCl_2$-MA in water resulted in a higher lift-off area of ≈50 $Å^2$. The surface pressure showed a smooth rise upon compression in the expanded regime of the Langmuir film ($\Pi < 16$ mN/m) and a uniform film was observed at $\Pi \approx 10$ mN/m in the BAM image. At $\Pi = 16$ mN/m, where the isotherm changes slope, a phase transition was observed in the BAM images associated with a change in conformation of $ODAH^+$ molecules at the water surface. Presumably the $ODAH^+$ molecules tend to lie down on the water surface at lower pressures ($\Pi <$ 16 mN/m) but stand up when the pressure is increased and give rise to a higher reflectivity in the BAM images. The steeper slope of the isotherm in the region $\Pi > 16$ mN/m supports this hypothesis since it indicates that the new phase is more rigid and more densely packed. The Langmuir film could not be compressed beyond a molecular area of 20 $Å^2$ and collapsed at $\Pi \approx 38$ mN/m.

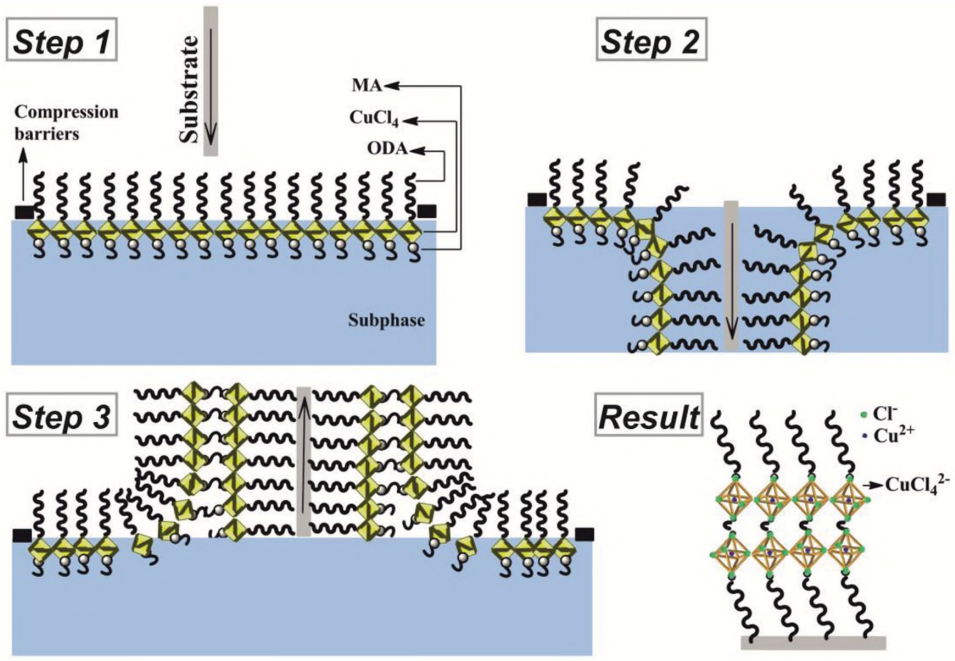

Figure 2. Schematics of the ordered Langmuir film floating at the subphase surface, built up from octadecyl ammonium chloride ($ODAH^+Cl^-$), $CuCl_2$ and methyl ammonium chloride (MA), and its transfer to a hydrophobic substrate during one dipping cycle at stable surface pressure.

2.2. Mechanism of Self-Assembly of the Hybrid Langmuir Film and Film Deposition

The isotherm behavior suggests the compression has induced the formation of a rigid $CuCl_x$-based sheet underneath the $ODAH^+$ molecular layer through electrostatic interaction. The proposed model of the hybrid Langmuir film sketched in **Figure 2** assumes that the $CuCl_x$-based layer is composed of Cl octahedra encaging the central Cu ions. Such a perovskite-like organic–inorganic superlattice structure has been reported for lead halide.[25,26] Formation of the octahedral environment around the central Cu ion becomes possible in the presence of 6 Cl atoms: 4 atoms share neighbouring atoms in-plane, one from the amphiphilic $ODAH^+Cl^-$ molecule and the last from the MA from the subphase. Such a hybrid structure has two types of organic spacers: $ODAH^+$ and MA, as sketched in Figure 2.

For deposition of a LB film, the Langmuir film was compressed at a rate of 30 cm^2 min^{-1} by the movable barrier until the desired surface pressure was reached and this pressure was kept constant during the whole deposition process. The compressed Langmuir film was allowed to stabilize for 30 min time before deposition.

LB films were deposited by vertical dipping of hydrophobic substrates into the subphase at a dipping speed of 5 mm/min. When a hydrophobic substrate is dipped into the subphase, the hydrophobic tails of $ODAH^+Cl^-$ interact with it during the downstroke, while during the upstroke the hydrophilic MA spacers interact; consequently a Y-type LB film[27] structure is formed at the end of the cycle (Figure 2). One dipping cycle (dipping down and retrieving the substrate from the subphase) hence corresponds to the deposition of two hybrid monolayers. In contrast to this film structure, bulk hybrids have a symmetric coordination of the organic ligands on both sides of the inorganic sheets.[2,3,24]

2.3. Corner-Shared $CuCl_4$-Based Inorganic Sheets

Robust magnetic properties observed in a bulk hybrid[2,4,28] originate from an inorganic $CuCl_4$-based backbone. The presence of such a backbone can be confirmed by X-ray photoelectron spectroscopy (XPS). We expect the crystal structure of the $CuCl_4$ layer in the LB film to be similar to that of the bulk hybrid and therefore the photoemission lines of N, Cu, and Cl to be similar.

The photoemission spectra of the Cu $2p_{3/2}$ core level region for a 16-layer-thick hybrid LB film and for a powder sample of a $CuCl_4$-based hybrid $CuCl_4(C_6H_5CH_2CH_2NH_3)_2$ are shown in the left panels of **Figure 3**. Both spectra show a shake-up satellite at the high binding energy side of the main peak which is a signature of Cu being in the +2 oxidation state.[29]

The Cu $2p_{3/2}$ spectrum for the bulk hybrid was fitted with a single component peaked at a binding energy (BE) of 934.4 eV which corresponds to Cu–Cl bonds within the octahedra; the shake-up satellite was fitted with two peaks in this case.

Fitting the Cu $2p_{3/2}$ line of the hybrid LB film revealed the presence of an additional lower binding energy component at 932.9 eV next to the one at 934.6 eV. This lower BE component also originates from Cu^{2+} ions as is evident from the additional corresponding satellite appearing at 941.5 eV. The satellite structure was fitted with one broad peak due to the limited signal to noise ratio in hybrid LB films. Similarly, the shake-up satellite with the main component at a binding energy of 934.6 eV was fitted with a single broad peak centred at 943.6 eV. The ratio between the main component peak

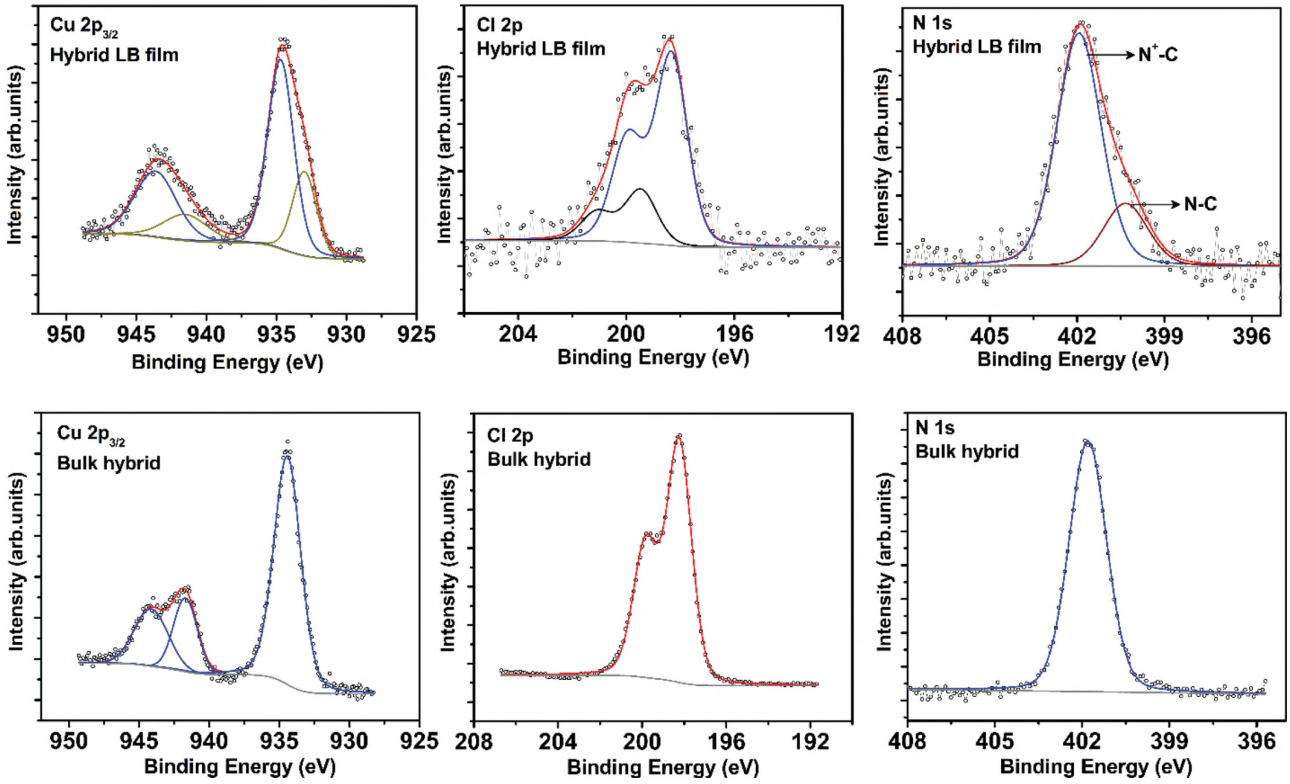

Figure 3. X-ray photoemission spectra of the Cu $2p_{3/2}$ (left panels), Cl 2p (middle panels) and N 1s (right panels) core level regions of a 16-layer-thick hybrid LB film (upper panels) and a $CuCl_4$-based bulk hybrid (lower panels) in powder form and fits to the experimental lines.

area and that of the corresponding satellite peak remains the same for the bulk hybrid and for the hybrid LB film.

A detailed scan of the Cl 2p core level region for the bulk hybrid is shown in Figure 3 (lower middle panel). The spectrum is fitted with one component peaked at 198.2 eV binding energy and corresponds to Cl bound to copper in the octahedron. However, in the Cl 2p core level spectrum of the hybrid film, shown in the top middle panel of Figure 3, an additional peak appears at 199.4 eV. The presence of two components in the Cu $2p_{3/2}$ and the Cl 2p spectra points to two phases in the film structure. About ~70% of the LB film has an inorganic layer structure similar to that of the bulk $CuCl_4$-based crystal hybrid. The second phase still contains Cu^{2+} and Cl^- as the inorganic parts but the bonding geometry must be different from the octahedral one since the lower binding energy of the additional component in the Cu $2p_{3/2}$ spectrum indicates a lower co-ordination. If we estimate the Cu^{2+} to Cl^- ratio for two phases from the intensities of the components in the photoemission spectra normalized with the sensitivity factors of each element including analyser transmission, we find Cu^{2+} : Cl^- = 1 : 3.96 ± 0.20 for the octahedral co-ordination and Cu^{2+} : Cl^- = 1 : 3.28 ± 0.20 for the second phase. Figure 3 also shows the photoemission spectra of the N 1s core level region for both the $CuCl_4$-based bulk hybrid and the hybrid LB film. The spectrum of the bulk hybrid consists of a single line assigned to the H_3N^+-C bond of the organic molecule. The spectrum of the N 1s core level region for the hybrid LB film showed an additional component at lower binding energy (400.3 eV) which indicates that ≈21% of the nitrogen species were de-protonated. Since protonated amine groups are required for the formation of $CuCl_4$-based inorganic sheets, the organic molecules with a de-protonated amine group are most likely involved in the formation of the second phase in the hybrid LB film. This suggests that a single-phase film could be achieved by improving the quality of the starting molecular building blocks.

2.4. Out-of-Plane Structure of the Hybrid LB Film

Figure 4 shows the scanning electron microscopy images collected on a 3-layer-thick hybrid LB film. This film thickness was achieved by removing the spread $ODAH^+Cl^-$ molecules from the air-water surface after the second dip before performing the upstroke. Two different phases giving different contrast can be observed: darker inclusions form a minority phase; based on the XPS results discussed above we suggest that this is the second phase with a Cu : Cl ratio of 1 : 3.28. The desired $CuCl_4$-based LB hybrid film (Cu : Cl ratio of ≈1 : 4) appears to be homogeneously deposited on the substrate. Since the Cu : Cl ratio in the second phase is smaller than the ratio in single layer bulk compounds, we propose a structural model of a corner-shared double layer of Cu_2Cl_7, analogous to double layer perovskites in bulk compounds.[30] A detailed atomic force microscopy study of this surface giving structural information on the second phase is presented in the Supporting Information and supports this model.

To gain insight into the structure of the film and to prove the high quality of the layer-by-layer deposition, X-ray diffraction studies were carried out on multilayer hybrid LB

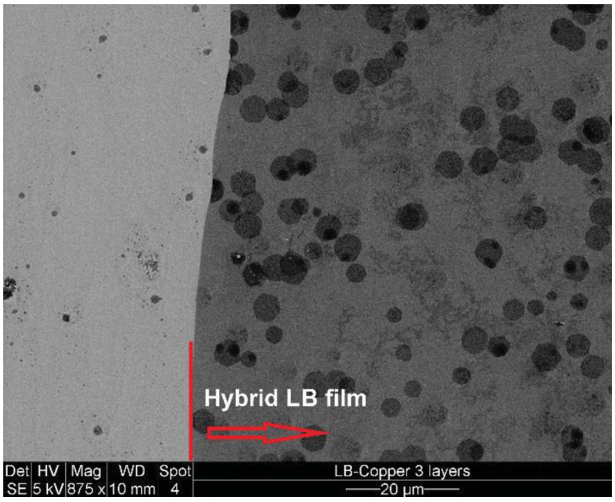

Figure 4. Scanning electron micrographs of two different areas of a 3-layer-thick hybrid LB film.

films. **Figure 5** shows the specular X-ray reflectivity of 8-layer-thick and 16-layer-thick hybrid LB films deposited at $\Pi = 30$ mN/m. Diffraction peaks as well as Kiessig fringes are observed for both films and provide evidence for a well-ordered layered structure. The length of the smallest periodic unit perpendicular to the film surface, d, can be calculated from the positions of the diffraction peaks using the Bragg formula. To determine the peak positions more precisely, the diffraction pattern was fitted with a linear combination of Gaussian and Lorentzian line shapes with a 75–25% ratio. The background taken in the fitting procedure was a polynomial function of 4th order. The value for d found for both the 8-layer-thick and the 16-layer-thick hybrid LB films was 54.5 ± 0.4 Å. This demonstrates that the crystal structure is independent of the number of layers. We note that the expected

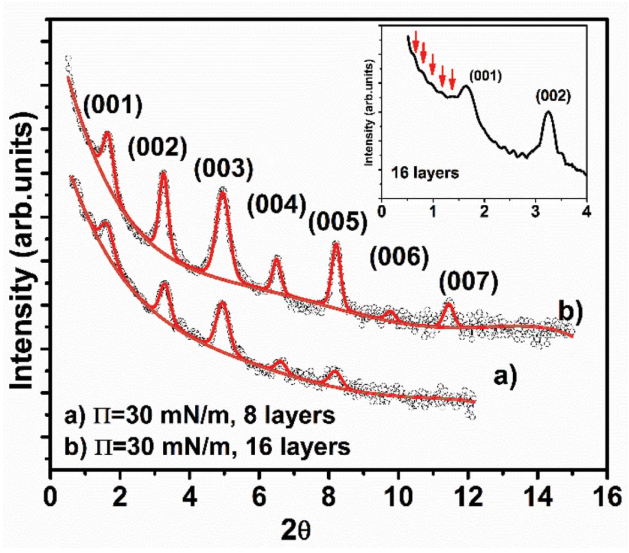

Figure 5. X-ray specular reflectivity patterns of multilayer hybrid LB films. The solid lines represent the corresponding fits. A magnified view of the data for a 16-layer-thick hybrid LB film deposited at a surface pressure of 30 mN/m (inset) shows both Kiessig fringes (indicated by arrows) and diffraction peaks.

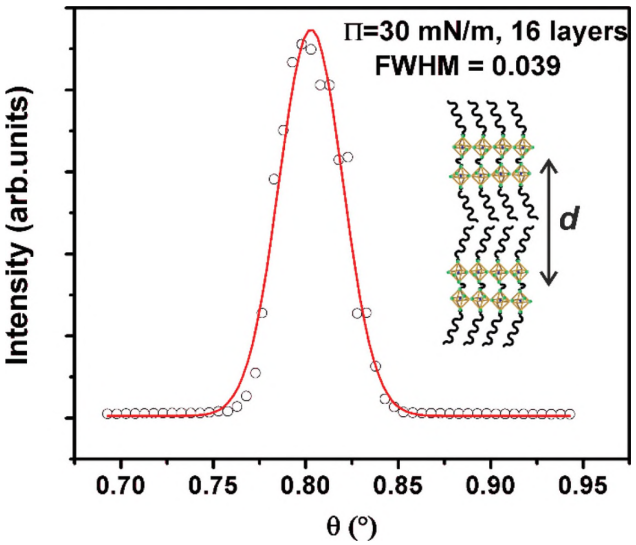

Figure 6. Rocking curve measured at the (001) diffraction peak position of a 16-layer-thick hybrid LB film deposited at a surface pressure of 30 mN/m. The red solid line represents a Gaussian fit to the data.

d value based on geometrical considerations is ≈62 Å (see Supporting Information), which is larger than the observed experimental value. Since the long $ODAH^+Cl^-$ molecules have a tendency to adopt a tilted conformation, the difference in d values most likely arises from the tilting of these molecules with respect to the film plane. The tilt angle would then be ≈58°.

The Kiessig fringes result from the interference of X-rays from two interfaces as a consequence of the angle-dependent phase shift, and their period is determined by the total thickness of the film.[31] The total thickness of these hybrid LB films determined from the Kiessig fringes is 219 Å for the 8-layer-thick film and 436 Å for the 16-layer-thick film. These values are within experimental accuracy in agreement with the repeat distance multiplied by the number of layers.

Figure 6 shows a rocking curve (θ-scan) measured at the (001) peak position in the out-of-plane orientation. A Gaussian fit to the rocking curve gives a FWHM of 0.039 ± 0.001° which indicates an outstandingly good parallel arrangement of layers within this multilayer hybrid LB film.

2.5. Ferromagnetism

Magnetism in bulk organic–inorganic hybrids arises from the transition metal ions in the inorganic perovskite sheets.[2,4,28,32] In hybrids that do not contain Cu, neighbouring cations are coupled antiferromagnetically in-plane via a superexchange path mediated by the Cl^- ions located between the metal ions.[2] The situation is different in Cu-containing hybrids; here the Cu^{2+} S = 1/2 ions are Jahn-Teller active and are involved in coherent orbital ordering, which leads to ferromagnetic coupling in the plane.[28,32] The in-plane elongation of the $CuCl_6$ octahedra in bulk hybrid crystals signals that the magnetic spin originates from the unoccupied Cu $d(x^2 - y^2)$ orbital. The ferromagnetic coupling always leads to 2D magnetic ordering in the planes and an

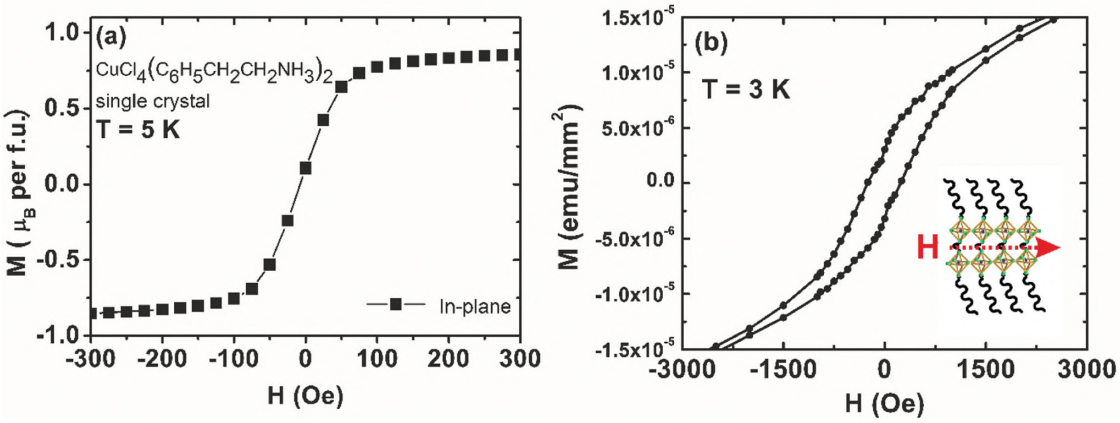

Figure 7. a) Magnetization versus field at 5 K for a $CuCl_4(C_6H_5CH_2CH_2NH_3)_2$ crystal measured in-plane (f.u. represents the $CuCl_4(C_6H_5CH_2CH_2NH_3)_2$ formula unit). b) Magnetic hysteresis loops at 3 K for a 1184-layer-thick hybrid LB film measured in-plane.

apparent 3D ferromagnetic state in most cases because of a divergence of the in-plane correlation length below T_c.[33,34]

Magnetization measurements were performed on a 1184-layer-thick hybrid LB film with a Quantum Design SQUID XL magnetometer. The large film thickness was necessary in order to obtain a measurable magnetic moment. The magnetization loop measured at 3 K with the field applied in the plane of the film shows the existence of a much enhanced coercive field in the LB hybrid film as compared to bulk ferromagnetic hybrid compounds (**Figure 7**). However, the ordering temperature remained the same in the hybrid LB film, when measured from *M–T* data (not shown here). The bulk hybrid material exhibits (glide) mirror symmetry in the Cu–Cl plane leading to symmetric coordination. However, in our hybrid LB films the Cu-Cl individual layers have an asymmetric coordination perpendicular to the layers because of the two different ligands – $ODAH^+Cl^-$ and MA. We propose that the enhanced coercivity originates from the asymmetric coordination of the Cu^{2+} spins by the $ODAH^+Cl^-$ and MA ligands, respectively. The magnetization loop does not saturate at high fields. We ascribe this to an antiferromagnetic (AF) contribution, given by the second phase, as discussed in the Supporting Information. We assign the structure of the second phase to a double layer of Cu–Cl octahedra in analogy with $K_3Cu_2F_7$,[30] which exhibits AF behavior.[35] A detailed study of the magnetic properties of this hybrid LB film is in progress and will be presented in a separate paper.

3. Conclusion

The synthesis of $CuCl_4$-based hybrid layers yields a new family of ferromagnetic thin films. These LB films are composed of a majority phase that has an inorganic layer structure similar to that of the $CuCl_4$-based bulk hybrid and a minority phase with a proposed corner-shared double layer of Cu_2Cl_7, analogous to double layer perovskites in bulk compounds. The LB films exhibit good crystallinity with smooth interfaces as evidenced from the X-ray diffraction studies. In contrast to bulk crystal growth, hybrid LB films can be tailored layer-by-layer, and are characterized by important differences in physical properties such as an enhancement of the coercive field. Such robust magnetic properties make these LB films promising candidates for applications in electronics. By using a different inorganic part in the LB synthesis, like FeCl-(phenylethylammonium)$_2$ which orders antiferromagnetically below 102 K,[36] higher ordering temperatures should be achievable. Moreover, with a well-chosen organic ligand one may also introduce other functional properties such as ferroelectricity.[6] Spintronics applications call for conductive thin films and this also seems within reach in these LB films since Arkenbout and coworkers[36,37] have shown that subliming TTF onto the surface of $CuCl_4(C_6H_5CH_2CH_2NH_3)_2$ crystals yields a conductive interface with an activation energy of 0.17 eV. Therefore one can conclude that organic–inorganic hybrid LB films with smooth and flat surfaces like those presented here offer excellent prospects for use as active layers in high quality electronic devices.

4. Experimental Section

Synthesis of $CuCl_4$-based Hybrid Langmuir-Blodgett Films: Octadecyl amine (>99%) was purchased from Fluka. Copper chloride ($CuCl_2$; 99.999%), methyl ammonium chloride (MA), and other chemical reagents of analytical grade were purchased from Sigma-Aldrich. To prepare octadecyl ammonium chloride ($ODAH^+Cl^-$), concentrated hydrochloric acid was slowly added to a stoichiometric octodecyl amine solution in ethanol. After reaction, the end product was filtered and re-crystallized with ethanol and chloroform. Ultra-pure ion-free water having a resistivity greater than 18 MΩ-cm was used for the preparation of the subphase. Surface pressure-molecular area (*Π–a*) isotherm measurements and deposition experiments were performed using a NIMA Technology thermostated LB trough. The temperature was kept at 21 °C during these experiments.

Synthesis of $CuCl_4(C_6H_5CH_2CH_2NH_3)_2$ Crystal Hybrid: Copper chloride ($CuCl_2$; 99.999%) and 2-phenylethylammoniumchloride (PEA; $C_6H_5CH_2CH_2NH_2Cl$) were purchased from Sigma-Aldrich. The $CuCl_2$ salt and PEA were mixed in a stoichiometric ratio. While the mixture was heated in a water bath of 50 °C, solvent (H_2O) was added until full solvation of the precursors was achieved. $CuCl_4(C_6H_5CH_2CH_2NH_3)_2$ crystals were recrystallized from the solution by slow evaporation of the solvent at 60 °C.

X-Ray Photoelectron Spectroscopy: 150 nm thick films of Au (purity 99.99%, Schöne Edelmetaal B.V.), grown on mica (Ted Paella, Inc.) as described in ref. [38] served as substrates for XPS measurements of $CuCl_4$-based bulk hybrids and LB hybrid films. Substrates were made hydrophobic prior to the LB film deposition.[39] XPS data were collected using a Surface Science SSX-100 ESCA instrument with a monochromatic Al Kα X-ray source ($h\nu$ = 1486.6 eV) operating at a base pressure of $\approx 3 \times 10^{-10}$ mbar. The spectra were recorded with an electron take-off angle of 37° with respect to the surface normal on the spot with a diameter of 600 µm. An electron flood gun providing 0.1 eV kinetic energy electrons in combination with a Mo grid mounted about 1 mm above the sample was used to compensate for sample charging. XPS spectra were analysed using the least-squares curve fitting program Winspec developed at the LISE laboratory, University of Namur, Belgium. The energy resolution was set to 1.26 eV. Binding energies are reported to a precision of ± 0.1 eV and referenced to the carbon 1s photoemission peak, centred at 285.2 eV.[40,41] Deconvolution of the spectra included background subtraction (Shirley baseline for Cu 2p and Cl 2p line, linear baseline for N 1s line because of the low signal-to-noise ratio of the latter) and fitting with a minimum number of peaks consistent with the structure of the molecules on a surface, taking into account the experimental resolution. The profile of the peaks was taken as a convolution of Gaussian and Lorentzian functions. The uncertainty in the peak intensity determination was 3% for nitrogen and chlorine, and 2% for copper. All measurements were carried out on freshly prepared samples. Three different spots were measured on each surface to check for reproducibility.

Scanning Electron Microscopy: For SEM, a 3-layer-thick film was deposited on the same substrate as for XPS measurements. Analysis was performed using a JEOL JSM-7000F microscope.

Atomic Force Microscopy: Si/SiO_2 wafers purchased from Silicon Quest International, USA, were employed for AFM studies. These were first cut into small pieces (usually 10 mm × 20 mm) and rendered hydrophobic[42] prior to film deposition. AFM images were recorded with a MultiMode 8 with ScanAsyst Microscope in tapping mode with TESP probes with spring constant $k = 42\ N \cdot m^{-1}$. Due to the fact that during prolonged scanning the tip was contaminated, for acquisition of each AFM picture a new probe was employed. The AFM images were analysed with the NanoScopeAnalysis software from Bruker.

X-Ray Diffraction Characterization: Diffraction measurements were performed at ambient conditions on 8-layer and 16-layer-thick hybrid LB films, deposited on a hydrophobic Si/SiO_2 substrate.[42] Out-of-plane X-ray reflectivity data were collected under ambient conditions using a Philips PANanalytical X'Pert MRD diffractometer. This diffractometer is equipped with a Cu Kα (λ = 1.5418 Å) radiation source (operated at 40 keV, 40 meV); a 0.25° divergence slit and a 0.125° antiscattering slit were employed. The 2θ scans were performed from 0.6° to 15° with a 0.02° step and a counting time of 15 s per step. Rocking curves were collected with a photon energy of 8 keV at the 001 peak position in the out-of-plane geometry at the SAXS-beamline at the ELETTRA synchrotron radiation facility in Trieste, Italy.[43]

Magnetic Characterization of the $CuCl_4$-based Hybrid LB Films: The magnetic properties were measured using a Quantum Design XL SQUID Magnetometer. The samples, a 1184-layer-thick $CuCl_4$-based LB film on a hydrophobic glass substrate [42] (0.1 mm thick Knittel Glass) or a $CuCl_4(C_6H_5CH_2CH_2NH_3)_2$ crystal, were mounted in a gelatin capsule, which was fixed in a plastic straw. The background signal was measured by mounting the clean substrate, prior to deposition, in a gelatin capsule fixed in a plastic straw. The background signal was negligibly small ($\approx 1.45 \times 10^{-6}$ emu/mm^2 at a temperature of 2 K and an applied field of 1 T).

Supporting Information

Film transfer characteristics, additional XPS spectra and morphology of hybrid LB film imaged by AFM are provided in the Supporting Information. This material is available from the Wiley Online Library or from the authors.

Acknowledgements

This research received financial support from the "Top Research School" program of the Zernike Institute for Advanced Materials under the Bonus Incentive Scheme (BIS) of the Netherlands' Ministry of Education, Science, and Culture.

[1] C. N. R. Rao, A. K. Cheetham, A. Thirumurugan, *J. Phys.: Condens. Matter* **2008**, *20*, 083202.
[2] P. Rabu, M. Drillon, *Adv. Eng. Mater.* **2003**, *5*, 189–210.
[3] D. B. Mitzi, *J. Chem. Soc., Dalton Trans.* **2001**, 1–12.
[4] L. J. de Jongh, W. D. Van Amstel, A. R. Miedema, *Physica* **1972**, *58*, 277–304.
[5] W. E. Estes, D. B. Losee, W. E. Hatfield, *J. Chem. Phys.* **1980**, *72*, 630.
[6] A. O. Polyakov, A. H. Arkenbout, J. Baas, G. R. Blake, A. Meetsma, A. Caretta, P. H. M. Van Loosdrecht, T. T. M. Palstra, *Chem. Mater.* **2012**, *24*, 133–139.
[7] D.-W. Fu, W. Zhang, H.-L. Cai, Y. Zhang, J.-Z. Ge, R.-G. Xiong, S. D. Huang, T. Nakamura, *Angew. Chem. Int. Ed.* **2011**, *50*, 11947–51.
[8] P. Jain, V. Ramachandran, R. J. Clark, H. D. Zhou, B. H. Toby, N. S. Dalal, H. W. Kroto, A. K. Cheetham, *J. Am. Chem. Soc.* **2009**, *131*, 13625–13627.
[9] E. Coronado, J. R. Galan-Mascaros, C. J. Gomez-Garcia, V. Laukhin, *Nat. Lett.* **2000**, *408*, 447–449.
[10] A. H. Arkenbout, T. Uemura, J. Takeya, T. T. M. Palstra, *Appl. Phys. Lett.* **2009**, *95*, 173104.
[11] C. Sanchez, B. Julián, P. Belleville, M. Popall, *J. Mater. Chem.* **2005**, *15*, 3559.
[12] C. Kagan, T. Breen, L. Kosbar, *Appl. Phys. Lett.* **2001**, *79*, 3536.
[13] A. C. Enríquez, M. G. F. Pérez, J. L. A. Sánchez, H. Höpfl, M. Parra-Hake, J. J. Campos-Gaxiola, *CrystEngComm* **2012**, *14*, 6146.
[14] J. H. Heo, S. H. Im, J. H. Noh, T. N. Mandal, C. Lim, J. A. Chang, Y. H. Lee, H. Kim, A. Sarkar, M. K. Nazeeruddin, M. Grätzel, S. Il Seok, *Nat. Photonics* **2013**, *7*, 486–491.
[15] J. Burschka, N. Pellet, S.-J. Moon, R. Humphry-Baker, P. Gao, M. K. Nazeeruddin, M. Grätzel, *Nature* **2013**, 3–7.
[16] C. R. Kagan, D. B. Mitzi, C. D. Dimitrakopoulos, *Science* **1999**, *286*, 945–947.
[17] D. B. Mitzi, *Chem. Mater.* **2001**, *13*, 3283–3298.
[18] Y. Ha, J. D. Emery, M. J. Bedzyk, H. Usta, A. Facchetti, T. J. Marks, *J. Am. Chem. Soc.* **2011**, *133*, 10239–50.

[19] M. Clemente-León, E. Coronado, A. Soriano-Portillo, E. Colacio, J. M. Dominguez-Vera, N. Galvez, R. Madueno, M. T. Martin-Romero, *Langmuir* **2006**, *22*, 6993–7000.
[20] M. Petruska, B. Watson, M. Meisel, D. Talham, *Chem. Mater.* **2002**, *14*, 2011–2019.
[21] K. Saruwatari, H. Sato, T. Idei, J. Kameda, A. Yamagishi, *J. Phys. Chem.* **2005**, *109*, 12410–12416.
[22] H. Sugai, T. Iijima, H. Masumoto, *Jpn. J. Appl. Phys.* **1999**, *38*, 5322–5325.
[23] M. Osada, K. Akatsuka, Y. Ebina, H. Funakubo, K. Ono, K. Takada, T. Sasaki, *ACS Nano* **2010**, *4*, 5225–5232.
[24] R. Willett, H. Place, M. Middleton, *J. Am. Chem. Soc.* **1988**, *110*, 8639–8650.
[25] L. Xu, X. Chen, L. Wang, Z. Sui, J. Zhao, B. Zhu, *Colloids Surf., A* **2005**, *257–258*, 457–460.
[26] M. Era, T. Kobayashi, M. Noto, *Curr. Appl. Phys.* **2005**, *5*, 67–70.
[27] M. C. Petty, *Langmuir-Blodgett Films*Cambridge University Press, Cambridge **1996**.
[28] M. Drillon, P. Panissod, *J. Magn. Magn. Mater.* **1998**, *188*, 93–99.
[29] N. S. Mclntyre, M. G. Cook, *Anal. Chem.* **1975**, *47*, 2208–2213.
[30] H. Manaka, Y. Miyashita, Y. Watanabe, T. Masuda, *J. Phys. Soc. Jpn.* **2007**, *76*, 044710.
[31] U. Pietsch, V. Holy, T. Baumbach, *High-resolution X-ray Scattering: From Thin Films to Lateral Nanostructures* Springer, New York **2004**.
[32] D. Khomskii, K. Kugel, *Solid State Commun.* **1973**, *13*, 763–766.
[33] L. J. de Jongh, P. Bloembergen, J. H. P. Colpa, *Physica* **1972**, *58*, 305–314.
[34] L. J. de Jongh, A. R. Miedema, *Adv. Phys.* **2001**, *50*, 947–1170.
[35] W. Brzezicki, A. M. Oleś, *Phys. Rev. B* **2011**, *83*, 214408.
[36] A. H. Arkenbout, *PhD Thesis*University of Groningen **2010**.
[37] A. H. Arkenbout, T. Uemura, J. Takeya, T. T. M. Palstra, *Appl. Phys. Lett.* **2009**, *95*, 173104.
[38] O. Ivashenko, H. Logtenberg, J. Areephong, A. C. Coleman, P. V. Wesenhagen, E. M. Geertsema, N. Heureux, B. L. Feringa, P. Rudolf, W. R. Browne, *J. Phys. Chem. C* **2011**, *115*, 22965–22975.
[39] Y. Habibi, I. Hoeger, S. S. Kelley, O. J. Rojas, *Langmuir* **2010**, *26*, 990–1001.
[40] J. F. Moulder, W. F. Stickle, P. E. Sobol, *Handbook of X-Ray Photoelectron Spectroscopy* Perkin-Elmer, Physical Electronics Division, Eden Prairie, MN **1993**.
[41] J. Díaz, G. Paolicelli, S. Ferrer, F. Comin, *Phys. Rev. B* **1996**, *54*, 8064–8069.
[42] G. l. Andreatta, Y. Jian Wang, F. Kay Lee, A. Polidori, P. Tong, B. Pucci, J.-J. Benattar, *Langmuir* **2008**, *24*, 6072–6078.
[43] H. Amenitsch, S. Bernstorff, M. Kriechbaum, D. Lombardo, H. Mio, M. Rappolt, P. Laggner, *J. Appl. Crystallogr.* **1997**, *30*, 872–876.